Nanoscale

Manipulating Topological Hall-like Signatures by Interface Engineering in Epitaxial Ruthenate/Manganite Heterostructures

Journal:	*Nanoscale*
Manuscript ID	NR-ART-05-2023-002407.R1
Article Type:	Paper
Date Submitted by the Author:	07-Sep-2023
Complete List of Authors:	Roy, Pinku; University at Buffalo, Department of Materials Design and Innovation; Los Alamos National Laboratory, CINT Zhang, Di; Purdue University, Materials Engineering; Los Alamos National Laboratory, Center for Integrated Nanotechnologies Mazza, Alessandro; Oak Ridge National Laboratory, Cucciniello, Nicholas; University at Buffalo Kunwar, Sundar; Los Alamos National Laboratory Zeng, Hao; State University of New York at Buffalo, Department of Physics Chen, Aiping; Los Alamos National Laboratory, Jia, Quanxi; University at Buffalo, Department of Materials Design and Innovation

Manipulating Topological Hall-like Signatures by Interface Engineering in Epitaxial Ruthenate/Manganite Heterostructures

Pinku Roy[1,2,*], Di Zhang[2], Alessandro R. Mazza[2], Nicholas Cucciniello[1,2], Sundar Kunwar[2], Hao Zeng[3], Aiping Chen[2,*], and Quanxi Jia[1,*]

[1]Department of Materials Design and Innovation, University at Buffalo - The State University of New York, Buffalo, NY 14260, USA

[2]Center for Integrated Nanotechnologies (CINT), Los Alamos National Laboratory, Los Alamos, New Mexico 87545, USA

[3]Department of Physics, University at Buffalo - The State University of New York, Buffalo, NY 14260, USA

**Email: pinkur@lanl.gov, apchen@lanl.gov , qxjia@buffalo.edu,*

Abstract: Topologically protected non-trivial spin textures (e.g. skyrmion) give rise to a novel phenomenon, called the topological Hall effect (THE), and have promising implications in future energy-efficient nanoelectronics and spintronic devices. Here, we have studied the Hall effect in $SrRuO_3/La_{0.42}Ca_{0.58}MnO_3$ (SRO/LCMO) bilayers. Our investigation suggests that pure SRO has hard and soft magnetic characteristics but the Anomalous Hall effect (AHE) in SRO is governed by the high coercivity phase. We have shown that the proximity effect of a soft magnetic LCMO on SRO plays a critical role in interfacial magnetic coupling and transport properties in SRO. With reducing the SRO thickness in the bilayer, the proximity effect becomes the dominant feature, enhancing the magnitude and temperature range of the THE-like signatures. The THE-like features in bilayers can be explained by a diffusive Berry phase transition model in the presence of an emergent magnetic state due to interface coupling. This work provides an alternative understanding of THE-like signatures and their manipulation in SRO-based heterostructures, bilayers and superlattices.

Keywords: Proximity effect, Anomalous Hall effect, Topological Hall effect, Inteface engineering, Heterostructure

Introduction:

Over the past few decades, theoretical and experimental advances in topological spin configurations in magnetic materials have opened up a new avenue of material science and fundamental physics. The vibrant topic has recently drawn considerable attention due to its potential application in the field of stable high-density nonvolatile memories as well as future energy-efficient nanoelectronics and spintronic devices[1,2]. Magnetic skyrmions are one of such topologically protected and stable spin configurations[3] which are observed in non-centrosymmetric lattice structures or interfacial symmetry-breaking heterostructures[4]. This topologically non-trivial chiral-spin texture with a whirling configuration can have a size of ~5 nm or less[5]. It is possible to manipulate skyrmion by much lower current densities on the order of $\sim 10^6$ A/m^2, compared to that required for driving ferromagnetic domain walls[6,7].

In a conventional ferromagnetic material, the alignment and orientation of spins are determined by exchange interactions and anisotropy, respectively. Whereas, Dzyaloshinskii-Moriya interaction (DMI)[8,9] in the presence of strong spin-orbit coupling (SOC) and broken inversion symmetry induces a relative tilt between neighboring spins. Competition between winding DMI and aligning exchange interactions is the reason behind the formation of two-dimensional whirling spin configurations (skyrmions).[10–13] Some other exotic spin configurations such as vortices[14], merons[15], bubbles[16], bobbers[17], and hopfions[18] are also possible to stabilize in a magnetic material by magnetostatic interactions[19], DMI[8,9], four spin exchange interactions[20] and frustrated exchange interactions[21,22].

Ordinary Hall effect (OHE) in a material is a consequence of Lorentz force which is proportional to the applied magnetic field. The Anomalous Hall effect (AHE) is another interesting phenomenon that is observed in ferromagnets and linked to magnetization[23]. The origin of intrinsic AHE is often described by the Berry phase in momentum space. Analogous to the Berry phase in momentum space, the real space Berry phase can also arise even without spin-orbit interaction in the presence of noncoplanar spin configuration with finite spin chirality[24]. An emergent magnetic field appears when charge carriers interact with these noncoplanar spin configurations[25–28]. The emergent magnetic field deflects the electrons perpendicular to the current direction and demonstrates interesting phenomena such as the Topological Hall effect by skyrmions[4,29,30]. THE appears as an additional contribution to the observed Hall signal. Therefore, the Hall resistivity in the presence of skyrmion in a magnetic material can be expressed as

$$\rho_H = \rho_{OHE} + \rho_{AHE} + \rho_{THE} \quad (1)$$

where the first term denotes the resistivity from the ordinary Hall effect due to majority charge carriers, the second term is from the anomalous Hall effect, proportional to magnetization and the third term is the additional resistivity due to THE. This additional contribution to the Hall resistivity appears as a distinct hump-like feature near the coercive field[31,32].

$SrRuO_3$, an itinerant ferromagnet, has been considered as a prototype for THE investigation. It's an ideal material system to explore novel topological physics[33,34] due to sizable spin-orbit coupling and multiple band crossings near the Fermi level[35]. In the past decade, most investigations on THE in SRO were focused on interface engineering by the proximity of heavy metal compounds[31,36–38], ferroelectric proximity[39–41], oxygen octahedra tilting[42,43] and even magnetic material proximity[44,45] to enhance the DMI. THE in SRO is highly controversial, the explanation of Hall anomaly based on two AHEs with opposite signs due to the presence of two magnetic phases refuses the presence of topological spin configuration[36,46–48]. In our previous article[49], we have shown that two Berry phases are responsible for THE-like feature but one of the Berry phases is not directly linked to the soft magnetic phase present in SRO. The origin of this second Berry phase over a limited range of temperature needs further investigation and in our present article, we have designed our experiment for further clarification and manipulation of THE-like feature in SRO. In this report, we have focused on stabilizing topological spin configuration based on necessary conditions[10] and investigated the results from a two-channel anomalous Hall effect perspective to figure out the governing mechanism for the Hall anomaly in our samples.

The Hamiltonian of DMI is described as

$$H_{DMI} = -\sum_{ij} \boldsymbol{D}_{ij} . S_i \times S_j \quad (2)$$

where $\boldsymbol{S}_i$ and $\boldsymbol{S}_j$ are the two neighboring spin vectors at the *i*th and *j*th sites respectively, and $\mathbf{D}_{ij}$ is the DMI vector. The magnitude of DMI depends on the cross-product of two neighboring spin vectors which are at a certain angle with each other, as evident from Eq. 2. Therefore, if we focus on obtaining non-collinearity by interface engineering approaches, the non-collinearity in spins is supposed to induce DMI at the interface. We believe interfacial coupling between two magnetic materials (ferromagnet (FM)/ferromagnet or ferromagnet/anti-ferromagnet (AFM) or ferromagnet/diamagnet) can provide significant noncolinear or canted spin structure at the interface. Hence, a heterostructure of two different magnetic materials can

be a source of DMI and topological spin configurations. Previously, the $SrRuO_3/La_{0.7}Sr_{0.3}MnO_3$ (FM/FM) bilayer has shown antiferromagnetic coupling at the interface and resulted THE-like feature[44,45]. In this work, we have selected SRO and $La_{0.42}Ca_{0.58}MnO_3$ (LCMO) as our model system, where LCMO composition lies above the 50% La substitution and can be antiferromagnet, ferromagnet or charge ordered phase depending on the oxidation state of Mn and temperature[50]. The selected composition is supposed to provide a competing magnetic state and hence a noncolinear or canted spin structure at the interface. We found that a soft magnetic phase of SRO originates due to interfacial coupling with poor ferromagnetic LCMO at the interface. Our study suggests such an interfacial coupling and the proximity effect between SRO and LCMO can be enhanced by reducing the thickness of SRO. Both, the temperature range and the magnitude of THE-like feature were found significantly enhanced with reducing SRO thickness.

Experimental: Epitaxial SRO/LCMO bilayer thin films on $SrTiO_3$ (STO) substrates with (001) orientation were grown by pulsed laser deposition with a KrF excimer laser (λ = 248 nm). Prior to the deposition, the STO substrates were annealed at 1000 ^oC for 2 hours in the air. The base pressure of the chamber was pumped down to the range of $\sim 1\times10^{-7}$ Torr. An optimized growth temperature of 700 ^oC and an oxygen pressure of 100 mTorr were used for the growth at a frequency of 2 Hz and 1.8 J/cm^2 laser fluence. To get uniform laser fluence, an imaged rectangle laser beam was focused onto the target[51]. The samples were cooled at the rate of 10 ^oC/min. At 450 ^oC, the chamber was filled with 200 Torr oxygen. The structural properties of all the films were characterized using a Panalytical X'pert PRO X-ray diffractometer with Cu Kα radiation. The microstructure was characterized by transmission electron microscopy (TEM) (FEI Titan 80-300 S/TEM with image-corrector operating at 300 kV), where the cross-sectional TEM samples were prepared by a standard manual grinding and thinning procedure followed by a final ion-polishing step (Gatan PIPS II 695 precision ion polishing system). Magnetic and magneto-transport properties were investigated using the vibrating sample magnetometer (VSM) and DC resistance setup from the Physical Property Measurement System (Quantum Design). Before the Hall measurement, the samples were wired in Hall bar geometry using indium metal, where the longitudinal direction measured the normal resistance and the transverse direction measured the Hall resistance. The Hall measurement has been carried out between -4T to 4T magnetic field. After each measurement, the sample has been warmed up to 200 K (above the T_c of SRO) to avoid any remanent magnetization in the film.

The out-of-plane *M-H* measurements were carried out at different temperatures within a field range from -3 T to 3 T.

Results and discussion:

XRD and TEM:

The magnetic and transport properties of thin films depend on their phase purity and crystallinity. Figure 1(a) shows the specular X-ray diffraction pattern of our SRO/LCMO bilayer films grown on $SrTiO_3$ (001) substrate. The presence of only (*00l)* reflections suggests pseudo cubic SRO and LCMO were deposited with the *c*-axis normal to the substrate surface. The out-of-plane lattice parameter (*c*) for SRO and LCMO were calculated from the diffraction pattern and found to be 3.98 Å and 3.75 Å, respectively. The reciprocal space map (RSM) around asymmetric (103) reflection indicates both SRO and LCMO layers were fully strained on STO (001) substrate. The strain status for these samples is similar and we believe the strain has limited impact on the property difference[52]. The thickness of SRO layers obtained from TEM was 16 nm, 8 nm and 5 nm respectively, whereas the LCMO thickness lies between 30 nm to 36 nm for all the bilayers. To simplify the discussion, we designate the bilayer samples as S16, S8, and S5, respectively. The high-resolution TEM (HR-TEM) images shown in Figures 1(c) and (d) confirm the highly crystalline and epitaxial quality of SRO and LCMO layers deposited on top of the STO substrate. The selected area electron diffraction (SAED) patterns shown in Figures 1(e) and (f) identify the epitaxial relationships as SRO(002)//LCMO(002)//STO(002) in both films.

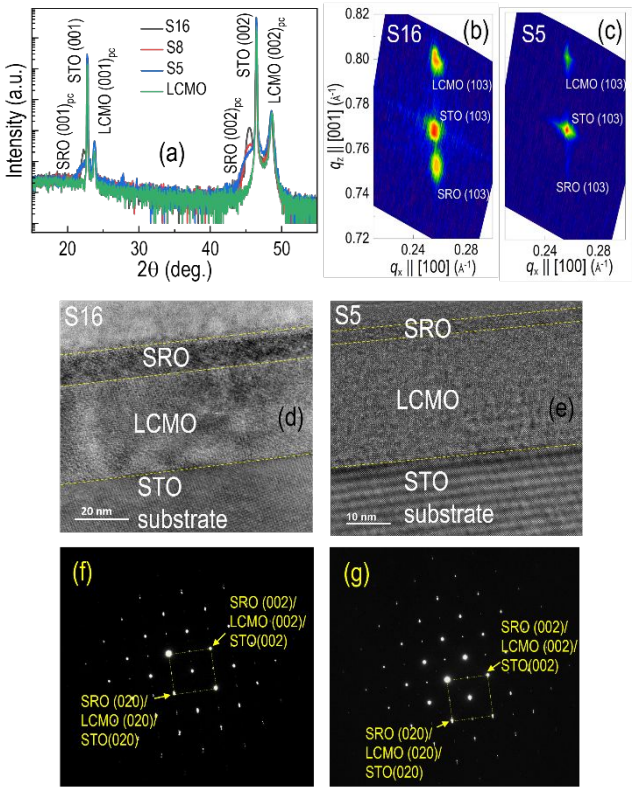

Figure 1: (a) X-ray θ-2θ diffraction patterns of SRO/LCMO bilayer films and a reference LCMO single phase film, (b) & (c) the RSM around STO (103) reflection for S16 and S5 samples, respectively. (d) & (e) HRTEM images and (f) & (g) SAED patterns of S16 and S5, respectively.

Transport properties:

The longitudinal resistivity (ρ_{xx}) and Hall resistivity (ρ_{xy}) of these bilayers were measured using conventional five-probe Hall bar geometry. The temperature dependence of the residual resistivity ratio (RRR = ρ_T/ρ_{10K}) is shown in Figure S1. The high RRR value of bilayers indicates highly crystalline films. All bilayer samples exhibit metallic behavior down to low temperatures. A cusp below 150 K corresponds to the paramagnetic to ferromagnetic transition (T_c) while cooling. This cusp for the bilayers was found to shift towards the lower temperature with decreasing SRO thickness which can be attributed to the reduced crystallinity of the film[53]. The experimental Hall resistivity data has been anti-symmetrized using $\rho_{xy} = [\rho_{xy}(H+) - \rho_{xy}(H-)]/2$ to avoid any magnetoresistance contribution. Magnetic field-dependent Hall resistivity, ρ_{xy}, at different temperatures was investigated to examine the thickness-dependent proximity effect on the electrical transport properties. Figures 2(a), (b) and (c) show the measured Hall resistivity of all three bilayer samples at different temperatures (all temperatures are shown in Figure S2). A square-shaped Hall resistivity within the ferromagnetic limit (below T_c) of SRO

is an indication of an anomalous Hall effect. The polarity of AHE changed between 80 K to 90 K for S16, which was reduced to between 70 K – 80 K for S8, as shown in Figure 2(d). The temperature at which polarity changes has been defined as T_S. Such a sign change in AHE has been attributed to the change in Berry curvature in momentum space[37,54]. It is clear that T_S reduces with reducing SRO thickness and in S5 (Figure 2(d)), such a polarity change never occurs as T_S reduces below the lowest measurement temperature (<10 K). Interestingly, all the bilayer samples exhibit THE-like features near the coercive field at certain temperatures. The temperature range at which THE feature appeared was also found to increase with decreasing thickness.

The sign of ρ_{THE} was always positive and varied systematically irrespective of the sign of AHE. The lack of correlation between the sign of THE-like feature and AHE suggests they have different origins. The enhanced THE-like feature as a function of the magnetic field at different temperatures in the bilayer can be visualized in Figures 2(e), (f) and (g). The color map in (*H, T*) space reveals that reducing thickness has an increasing effect on both magnitudes of ρ_{THE} as well as the magnetic field range over which THE-like feature is observed. Although the temperature for THE-like feature reduced with thickness, the enhanced range of the magnetic field suggests the thermodynamic stability of the responsible specific magnetic state has been amplified by reducing the SRO thickness. To confirm the effect, we also deposited single-layer SRO films (16 nm and 5 nm) at the same growth conditions as the bilayers. Similar Hall measurements show no THE-like feature (Figure S6). These results indicate THE-like feature in bilayers is related to the proximity of the LCMO layer, which is enhanced with decreasing SRO thickness.

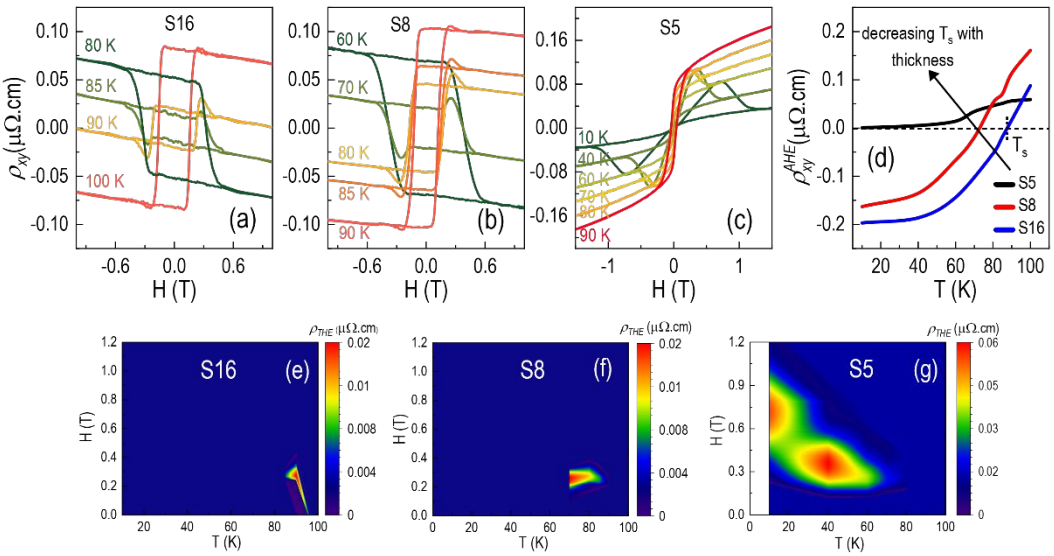

Figure 2: (a), (b), and (c) the Hall resistivity of S16, S8, and S5, respectively, (d) the change in sign of anomalous Hall effect and the effect of thickness on shifting the sign change temperature (T_s). (e), (f) and (g) show the change in ρ_{THE} in *H vs T* space for S16, S8, and S5, respectively.

We investigated the relation between ρ_{xy} vs ρ_{xx} to figure out the scattering mechanism(s) in these bilayers, as shown in Figure S3. The scaling relation suggests a combination of intrinsic (Berry phase) and extrinsic (skew scattering and/or side jump) mechanisms are contributing to the AHE below the sign change temperature. Beyond T_s, a deviation from the obtained scaling relation suggests the scattering mechanism has been changed or modified after the Berry phase transition but no conclusive evidence regarding the THE-like feature was obtained.

Magnetic properties:

To decipher the origin of THE-like feature in these bilayers, investigation of the magnetic properties and its correlation with AHE is important. Figure 3 demonstrates the out-of-plane magnetization of S16, S8, S5, pure 5 nm SRO single layer, and LCMO single layer on STO (001) substrates at different temperatures (all results are shown in Figure S4). Thicker SRO bilayers (S16 and S8) showed a two-step magnetic hysteresis at low temperatures, indicating two magnetic phase contributions. Out of these two phases, one is hard magnetic having higher H_C, whereas, the second phase is soft magnetic (low H_C). The magnetic measurement of pure LCMO film reveals its soft magnetic behavior over the entire temperature range, which suggests that magnetization in the bilayer is a collective behavior of SRO and LCMO. Moreover, the temperature-dependent magnetization in thick bilayers was found to undergo a transition from a mixture of hard and soft magnetic phases to a soft magnetic phase at high temperatures. Interestingly, a similar hard-soft magnetic to soft magnetic phase transition has been observed in single-layer SRO at high temperature. When the same thickness of SRO is coupled to LCMO, the bilayer (S5) does not show two-step magnetic hysteresis (the present magnetic phase was soft over the entire temperature range). The comparison of magnetic properties in single-layer and bilayer SRO films reveals both, the temperature and thickness of SRO in the bilayer influence the magnetic phase transition (i.e. hard-soft to soft magnetic).

It is important to note here that THE-like feature was observed in the vicinity of temperatures where the hard-soft to soft magnetic transition is taking place in S16 and S8. Moreover, THE-like feature was more prominent and existed over a broad range of temperatures in S5 where SRO is in a soft magnetic state by mimicking LCMO. Therefore, our comparison of Hall resistivity and magnetic properties in these single-layer and bilayer SRO films indicates the

THE-like feature is a result of interface coupling between SRO and LCMO. In addition to that, the hard-soft magnetic to a soft magnetic phase transition provides the necessary magnetic phase for a diffuse Berry phase transition. The necessary magnetic phase can be manipulated in SRO by controlling the temperature and its thickness in the proximity of soft magnetic LCMO.

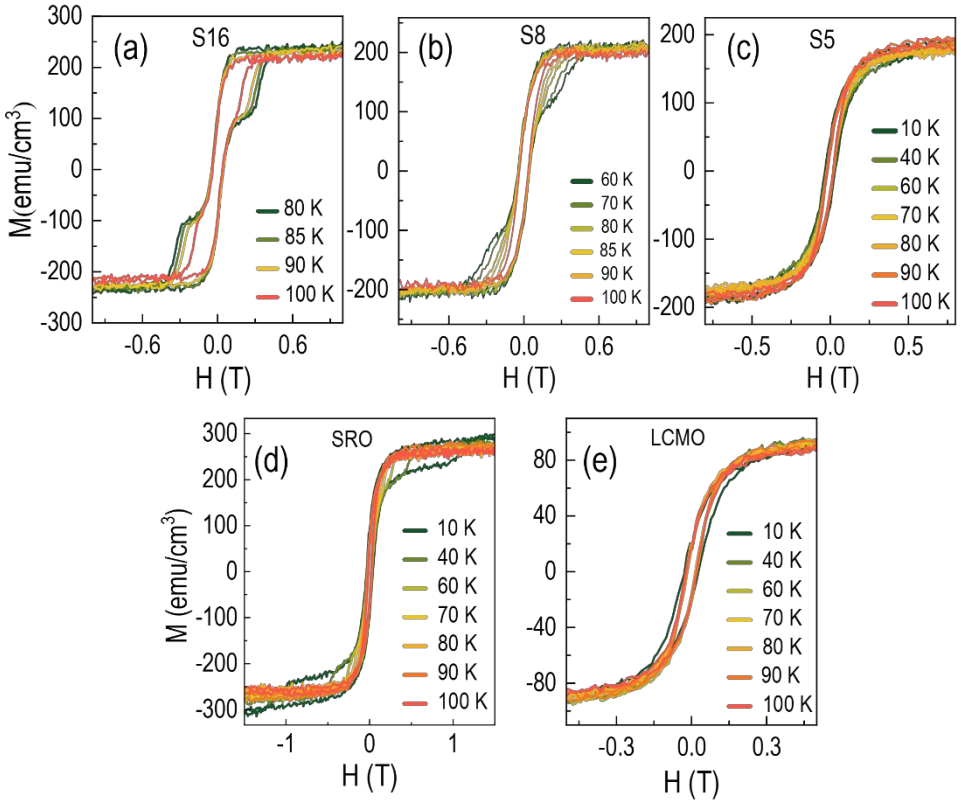

Figure 3: Out-of-plane M-H plots of (a) S16, (b) S8, (c) S5, (d) 5 nm pure SRO, and (e) pure LCMO respectively, at different temperatures.

Discussion:

For all the bilayer samples, regardless of mixed or single phase behavior, the hump feature in Hall resistivity was fitted by two AHEs with opposite polarity. This allows for a direct comparison of the Hall components with potential counterparts in the magnetization measurements. We found at low temperatures the high H_c magnetic phase is solely responsible for the AHE. The only discrepancy occurs near the T_S, where the hump feature appeared. Two AHEs with opposite polarity generate similar hump features in both samples. These two AHEs also provide the necessary information about their magnetic counterpart which are responsible for THE-like feature. The comparison between two AHEs and present magnetic phases around

T_S reveals that the high H_C magnetic phase is responsible for one of the AHE but the origin of the second AHE is not from the low H_c magnetic phase, present in the bilayer. We mapped the two magnetic coercivities, H_C's of two AHEs and the magnetic field at which the magnetoresistance peak appeared (H_p-MR) as a function of temperature. The comparison between these characteristic fields is shown in Figure 4. In the figure, we termed the high H_C magnetic phase as P1 and the low H_C magnetic phase as P2. It is interesting to note in Figures 4(d) and (e) that the coercivity of Hall resistivity, H_C of the P1 phase and H_p-MR matches quite well until the THE-like feature appears in the system. The comparison also suggests that H_p-MR always represents the hard-magnetic phase. When the THE-like feature appears, AHE1 and H_p-MR still seem to follow the high H_c phase but AHE2 does not have any correlation with the hard or soft magnetic phases observed in the *M-H* measurement. A similar approach of using two AHEs to fit the Hall resistivity in S5 was adopted to investigate the magnetic counterpart of hypothetical AHEs (Figure 4 (f)). The comparison of peak magnetoresistance (H_p-MR) for S16, S8, and S5 reveals that the behavior of sample S5 is still hard-magnetic during the transport measurement. However, the non-contact *M-H* measurement suggests S5 as a soft magnet, which is possibly a thickness effect as we have seen similar behavior in S8 beyond 80 K but not in S16. We can also see in S5 that AHE2 appears to originate from the high coercivity phase but AHE1 does not have a direct relation to the soft magnetic phase. Such a lack of correlation between soft magnetic phase(s) and an AHE to describe the THE-like feature in all the samples indicates the origin of the second AHE is not directly related to the soft magnetic phase observed in the *M-H* measurement. The appearance of the second AHE within a narrow temperature window suggests the presence of an emergent magnetic phase, most likely at the interface. The hump feature in SRO[42,55–57] and other material systems such as MnSi[29], $Mn_{1.5}PtSn$[58], Mn_2CoAl[59], $Cr_{1.2}Te_2$[60] has been attributed to topological Hall effect due to noncoplanar spin texture. Nevertheless, an alternative explanation for the THE feature based on two AHEs with opposite polarity makes its topological origin doubtful. These two AHEs were linked to magnetic inhomogeneity in SRO[46–48,61]. SRO having two magnetic phases is well accepted among the scientific community[62–65]. In our previous work, we proposed a phenomenological model to explain the THE-like feature in single-layer SRO thin films[49]. Our results suggest that a diffusive Berry phase transition model is more appropriate. In this model, the magnetic phase with relatively higher coercivity (H_C) contributes to AHE, which has a sign

change near T_S and a certain magnetic state bears two Berry phases, with positive and negative signs. Such a model and observations also match with the results in this work.

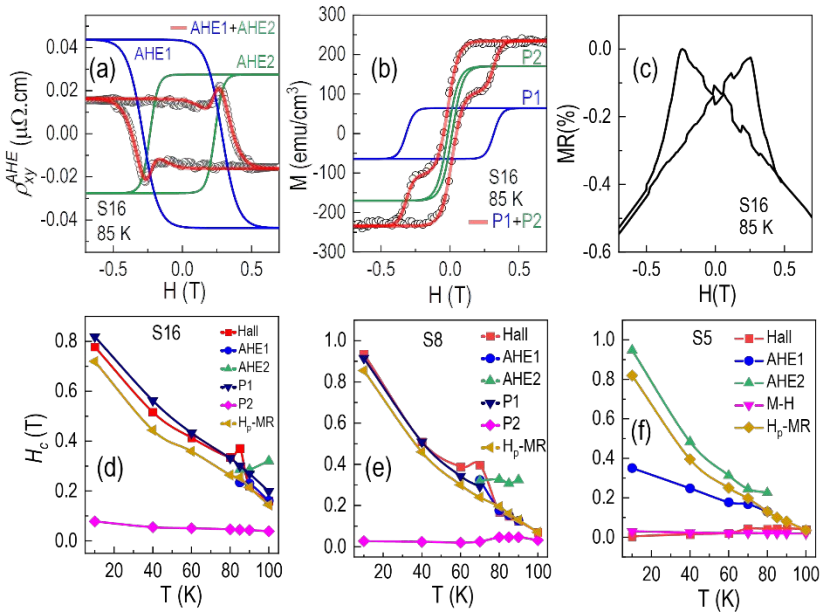

Figure 4: (a) An example of two-channel AHE fitting of ρ_{xy} for S16 at 85 K, (b) magnetic hysteresis as a sum of two magnetic contributions with hard and soft behavior respectively, (c) corresponding magnetoresistance at 85 K for sample S16 (all temperatures are shown in Figure S4.) and (d-f) the coercivities of Hall, fitted AHE, magnetism and magnetoresistance obtained between 10 K to 100 K for samples S16, S8 and S5, respectively.

Our thickness-dependent study of Hall resistivity has produced a consistent topological Hall effect feature which is enhanced with decreasing thickness. The sign of ρ_{THE} was always positive and varied systematically irrespective of the sign of AHE. Moreover, THE-like feature was present in the bilayer samples with both dual magnetic phase (S16 and S8) and single magnetic phase (S5) characteristics. Similar dual magnetic phases were observed in single-layer SRO films but the absence of THE-like feature suggests the necessary magnetic state to give rise to hump-like feature in SRO originates due to the proximity effect of LCMO. This responsible magnetic state in SRO can be stabilized by controlling its thickness when the SRO is interfacially coupled to a soft magnetic material. We have provided a schematic of the possible mechanism for the appearance of an emergent magnetic phase, responsible for the THE-like feature at the SRO/LCMO interface, shown in Figure 5. To understand the origin of the emergent magnetic phase, we first describe the concept of exchange coupling between two magnetic materials. The absence of coupling between two magnetic materials gives rise to two-step features in the magnetic hysteresis, as shown in Figure 5(a). When SRO is deposited on top of a bare STO substrate, magnetic SRO is in proximity with a non-magnetic STO. As a

result, a soft magnetic phase arises at the interface. The lack of coupling between this soft magnetic phase and the bulk hard magnetic phase gives rise to a two-step feature in magnetic hysteresis, similar to Figure 5(a). The scenario is different in the presence of exchange coupling between two magnetic materials. The combination of a hard and soft magnetic phases gives rise to a single-step magnetic hysteresis with coercivity lying in between the hard and soft magnetic phases in the presence of exchange coupling, as shown in Figure 5(b). When SRO is in close proximity with a soft magnetic LCMO, a soft magnetic phase of SRO develops at the interface, which we can identify from the *M-H* measurement. Initially, this soft magnetic phase remains decoupled with the hard magnetic phase of SRO and it shows a two-step magnetic hysteresis. It is important to mention that the soft magnetic contribution to the Hall resistivity was absent at low temperatures, otherwise a step feature or THE-like feature must have appeared in the ρ_{xy}. As the temperature increases, the bulk SRO undergoes a hard-soft (H-S) magnetic to a soft magnetic phase transition. In this condiction, the interfacial layer is surrounded by H-S SRO and soft magnetic LCMO and due to exchange coupling between SRO and LCMO the interfacial layer gives rise to an emergent magnetic phase. The phenomena of exchange coupling and emergent magnetic phase can be well understood by Figures 5(d) and (e). This emergent magnetic phase holds the Berry phases with opposite polarity to give rise to THE-like feature. The effect of thickness reduction of SRO in the bilayer can be understood from Figure 5(e), where such a magnetic state is spread deep inside the thin SRO layer and the entire film holds the characteristics of the interfacial state. The Berry phase transition and coexistence of two Berry phases due to an emergent magnetic phase can be manipulated over wide temperature ranges by reducing the thickness of SRO in the bilayer. The phenomena are described in Figure 5(f), where pure SRO undergoes a sharp Berry phase transition at T_S but a diffuse Berry phase transition state exists only in the presence of soft magnetic LCMO. Reducing the thickness of SRO affects both T_S and the width of diffusive Berry phase transition.

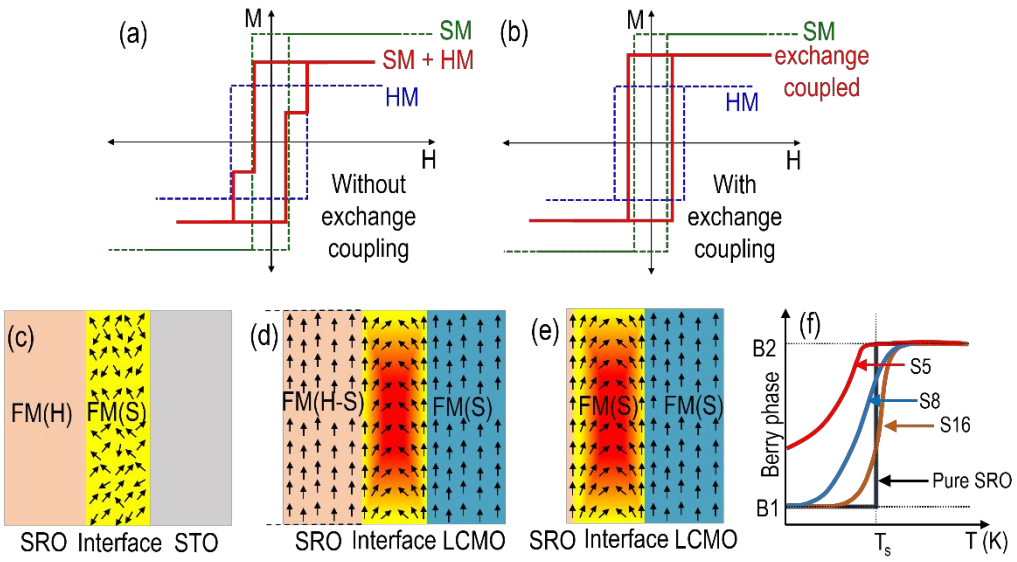

Figure 5: Schematic description of (a) Magnetic hysteresis (two-step feature) resulting from the absence of exchange coupling between two magnetic phases (b) magnetic hysteresis in presence of exchange coupling between two magnetic phases, (c) presence of uncoupled hard magnetic (FM (H)) and soft magnetic (FM (S)) phases. (d) and (e) the interfacial magnetic state for thick and thin SRO bilayers in SRO/LCMO heterostructure, and (f) schematic illustration of the role of SRO thickness on the sign change of Hall resistivity and two Berry phase coexistence.

Conclusion:

In summary, we have demonstrated that SRO behaves as a mixture of hard and soft magnetic phases in a heterostructure. Hall resistivity measurements indicate that the high coercivity magnetic phase of SRO is solely responsible for AHE, whereas the THE-like feature in SRO is only observed when it is in proximity with LCMO. Magnetic measurements reveal that the THE-like feature is observed in the vicinity of a hard-soft magnetic to a soft magnetic phase transition. Moreover, fitting of the THE-like feature in the Hall resistivity with two AHE model suggests the magnetic counterpart of the second AHE with the opposite sign is not directly related to the soft magnetic phase. This suggests the proximity of LCMO plays a critical role in manipulating the magnetic behaviour of SRO and hence its transport properties. The THE-like feature can be explained by a diffuse Berry phase transition model in the presence of an exchange-coupled emergent magnetic phase. Such a magnetic state, bearing two opposite Berry phases can be stabilized over a broad range of temperatures by reducing the thickness of SRO in the bilayer. Although the Hall effect and magnetic measurements confirm the presence of a distinct magnetic state as the origin of the THE-like feature in the bilayers, the exact nature of

such a magnetic phase is still unknown and needs advanced characterization to probe its spin configuration.

Notes

The authors declare no competing financial interest.

Acknowledgement

The work at the University at Buffalo (UB) was funded by the U.S. National Science Foundation (ECCS-1902623). P. R. and Q. X. J. acknowledge the CINT Users Program. The work at Los Alamos National Laboratory was supported by the NNSA's Laboratory Directed Research and Development Program and was performed, in part, at the Center for Integrated Nanotechnologies (CINT), an Office of Science User Facility operated for the U.S. Department of Energy Office of Science. Los Alamos National Laboratory, an affirmative action equal opportunity employer, is managed by Triad National Security, LLC for the U.S. Department of Energy's NNSA, under contract 89233218CNA000001. P. Roy and A. Chen acknowledge the support from LANL Seaborg Institute.

References:

(1) Chen, S.; Yuan, S.; Hou, Z.; Tang, Y.; Zhang, J.; Wang, T.; Li, K.; Zhao, W.; Liu, X.; Chen, L.; Martin, L. W.; Chen, Z. Recent Progress on Topological Structures in Ferroic Thin Films and Heterostructures. *Advanced Materials* **2021**, *33* (6), 2000857. https://doi.org/10.1002/adma.202000857.

(2) Seidel, J. Nanoelectronics Based on Topological Structures. *Nature Mater* **2019**, *18* (3), 188–190. https://doi.org/10.1038/s41563-019-0301-z.

(3) Rößler, U. K.; Bogdanov, A. N.; Pfleiderer, C. Spontaneous Skyrmion Ground States in Magnetic Metals. *Nature* **2006**, *442* (7104), 797–801. https://doi.org/10.1038/nature05056.

(4) Kurumaji, T.; Nakajima, T.; Hirschberger, M.; Kikkawa, A.; Yamasaki, Y.; Sagayama, H.; Nakao, H.; Taguchi, Y.; Arima, T.; Tokura, Y. Skyrmion Lattice with a Giant Topological Hall Effect in a Frustrated Triangular-Lattice Magnet. *Science* **2019**. https://doi.org/10.1126/science.aau0968.

(5) Wang, X. S.; Yuan, H. Y.; Wang, X. R. A Theory on Skyrmion Size. *Commun Phys* **2018**, *1* (1), 1–7. https://doi.org/10.1038/s42005-018-0029-0.

(6) Jonietz, F.; Mühlbauer, S.; Pfleiderer, C.; Neubauer, A.; Münzer, W.; Bauer, A.; Adams, T.; Georgii, R.; Böni, P.; Duine, R. A.; Everschor, K.; Garst, M.; Rosch, A. Spin Transfer Torques in MnSi at Ultralow Current Densities. *Science* **2010**. https://doi.org/10.1126/science.1195709.

(7) Yu, X. Z.; Kanazawa, N.; Zhang, W. Z.; Nagai, T.; Hara, T.; Kimoto, K.; Matsui, Y.; Onose, Y.; Tokura, Y. Skyrmion Flow near Room Temperature in an Ultralow Current Density. *Nat Commun* **2012**, *3* (1), 988. https://doi.org/10.1038/ncomms1990.

(8) Dzyaloshinsky, I. A Thermodynamic Theory of "Weak" Ferromagnetism of Antiferromagnetics. *Journal of Physics and Chemistry of Solids* **1958**, *4* (4), 241–255. https://doi.org/10.1016/0022-3697(58)90076-3.

(9) Moriya, T. Anisotropic Superexchange Interaction and Weak Ferromagnetism. *Phys. Rev.* **1960**, *120* (1), 91–98. https://doi.org/10.1103/PhysRev.120.91.

(10) Nagaosa, N.; Tokura, Y. Topological Properties and Dynamics of Magnetic Skyrmions. *Nature Nanotech* **2013**, *8* (12), 899–911. https://doi.org/10.1038/nnano.2013.243.
(11) Mühlbauer, S.; Binz, B.; Jonietz, F.; Pfleiderer, C.; Rosch, A.; Neubauer, A.; Georgii, R.; Böni, P. Skyrmion Lattice in a Chiral Magnet. *Science* **2009**. https://doi.org/10.1126/science.1166767.
(12) Yu, X. Z.; Onose, Y.; Kanazawa, N.; Park, J. H.; Han, J. H.; Matsui, Y.; Nagaosa, N.; Tokura, Y. Real-Space Observation of a Two-Dimensional Skyrmion Crystal. *Nature* **2010**, *465* (7300), 901–904. https://doi.org/10.1038/nature09124.
(13) Soumyanarayanan, A.; Raju, M.; Gonzalez Oyarce, A. L.; Tan, A. K. C.; Im, M.-Y.; Petrović, A. P.; Ho, P.; Khoo, K. H.; Tran, M.; Gan, C. K.; Ernult, F.; Panagopoulos, C. Tunable Room-Temperature Magnetic Skyrmions in Ir/Fe/Co/Pt Multilayers. *Nature Mater* **2017**, *16* (9), 898–904. https://doi.org/10.1038/nmat4934.
(14) Chmiel, F. P.; Waterfield Price, N.; Johnson, R. D.; Lamirand, A. D.; Schad, J.; van der Laan, G.; Harris, D. T.; Irwin, J.; Rzchowski, M. S.; Eom, C.-B.; Radaelli, P. G. Observation of Magnetic Vortex Pairs at Room Temperature in a Planar α-Fe2O3/Co Heterostructure. *Nature Mater* **2018**, *17* (7), 581–585. https://doi.org/10.1038/s41563-018-0101-x.
(15) Yu, X. Z.; Koshibae, W.; Tokunaga, Y.; Shibata, K.; Taguchi, Y.; Nagaosa, N.; Tokura, Y. Transformation between Meron and Skyrmion Topological Spin Textures in a Chiral Magnet. *Nature* **2018**, *564* (7734), 95–98. https://doi.org/10.1038/s41586-018-0745-3.
(16) Kittel, C. Physical Theory of Ferromagnetic Domains. *Rev. Mod. Phys.* **1949**, *21* (4), 541–583. https://doi.org/10.1103/RevModPhys.21.541.
(17) Zheng, F.; Rybakov, F. N.; Borisov, A. B.; Song, D.; Wang, S.; Li, Z.-A.; Du, H.; Kiselev, N. S.; Caron, J.; Kovács, A.; Tian, M.; Zhang, Y.; Blügel, S.; Dunin-Borkowski, R. E. Experimental Observation of Chiral Magnetic Bobbers in B20-Type FeGe. *Nature Nanotech* **2018**, *13* (6), 451–455. https://doi.org/10.1038/s41565-018-0093-3.
(18) Shinjo, T.; Okuno, T.; Hassdorf, R.; Shigeto, † K.; Ono, T. Magnetic Vortex Core Observation in Circular Dots of Permalloy. *Science* **2000**. https://doi.org/10.1126/science.289.5481.930.
(19) Ezawa, M. Giant Skyrmions Stabilized by Dipole-Dipole Interactions in Thin Ferromagnetic Films. *Phys. Rev. Lett.* **2010**, *105* (19), 197202. https://doi.org/10.1103/PhysRevLett.105.197202.
(20) Heinze, S.; von Bergmann, K.; Menzel, M.; Brede, J.; Kubetzka, A.; Wiesendanger, R.; Bihlmayer, G.; Blügel, S. Spontaneous Atomic-Scale Magnetic Skyrmion Lattice in Two Dimensions. *Nature Phys* **2011**, *7* (9), 713–718. https://doi.org/10.1038/nphys2045.
(21) Zhang, X.; Xia, J.; Zhou, Y.; Liu, X.; Zhang, H.; Ezawa, M. Skyrmion Dynamics in a Frustrated Ferromagnetic Film and Current-Induced Helicity Locking-Unlocking Transition. *Nat Commun* **2017**, *8* (1), 1717. https://doi.org/10.1038/s41467-017-01785-w.
(22) Leonov, A. O.; Mostovoy, M. Multiply Periodic States and Isolated Skyrmions in an Anisotropic Frustrated Magnet. *Nat Commun* **2015**, *6* (1), 8275. https://doi.org/10.1038/ncomms9275.
(23) Nagaosa, N.; Sinova, J.; Onoda, S.; MacDonald, A. H.; Ong, N. P. Anomalous Hall Effect. *Rev. Mod. Phys.* **2010**, *82* (2), 1539–1592. https://doi.org/10.1103/RevModPhys.82.1539.
(24) Onoda, M.; Tatara, G.; Nagaosa, N. Anomalous Hall Effect and Skyrmion Number in Real and Momentum Spaces. *J. Phys. Soc. Jpn.* **2004**, *73* (10), 2624–2627. https://doi.org/10.1143/JPSJ.73.2624.
(25) Bansil, A.; Lin, H.; Das, T. Colloquium: Topological Band Theory. *Rev. Mod. Phys.* **2016**, *88* (2), 021004. https://doi.org/10.1103/RevModPhys.88.021004.
(26) Emori, S.; Bauer, U.; Ahn, S.-M.; Martinez, E.; Beach, G. S. D. Current-Driven Dynamics of Chiral Ferromagnetic Domain Walls. *Nature Mater* **2013**, *12* (7), 611–616. https://doi.org/10.1038/nmat3675.
(27) Grytsiuk, S.; Hanke, J.-P.; Hoffmann, M.; Bouaziz, J.; Gomonay, O.; Bihlmayer, G.; Lounis, S.; Mokrousov, Y.; Blügel, S. Topological–Chiral Magnetic Interactions Driven by Emergent Orbital Magnetism. *Nat Commun* **2020**, *11* (1), 511. https://doi.org/10.1038/s41467-019-14030-3.

(28) Schulz, T.; Ritz, R.; Bauer, A.; Halder, M.; Wagner, M.; Franz, C.; Pfleiderer, C.; Everschor, K.; Garst, M.; Rosch, A. Emergent Electrodynamics of Skyrmions in a Chiral Magnet. *Nature Phys* **2012**, *8* (4), 301–304. https://doi.org/10.1038/nphys2231.
(29) Neubauer, A.; Pfleiderer, C.; Binz, B.; Rosch, A.; Ritz, R.; Niklowitz, P. G.; Böni, P. Topological Hall Effect in the A Phase of MnSi. *Phys. Rev. Lett.* **2009**, *102* (18), 186602. https://doi.org/10.1103/PhysRevLett.102.186602.
(30) Vistoli, L.; Wang, W.; Sander, A.; Zhu, Q.; Casals, B.; Cichelero, R.; Barthélémy, A.; Fusil, S.; Herranz, G.; Valencia, S.; Abrudan, R.; Weschke, E.; Nakazawa, K.; Kohno, H.; Santamaria, J.; Wu, W.; Garcia, V.; Bibes, M. Giant Topological Hall Effect in Correlated Oxide Thin Films. *Nature Physics* **2019**, *15* (1), 67–72. https://doi.org/10.1038/s41567-018-0307-5.
(31) Matsuno, J.; Ogawa, N.; Yasuda, K.; Kagawa, F.; Koshibae, W.; Nagaosa, N.; Tokura, Y.; Kawasaki, M. Interface-Driven Topological Hall Effect in $SrRuO_3$-$SrIrO_3$ Bilayer. *Sci. Adv.* **2016**, *2* (7), e1600304. https://doi.org/10.1126/sciadv.1600304.
(32) Ohuchi, Y.; Matsuno, J.; Ogawa, N.; Kozuka, Y.; Uchida, M.; Tokura, Y.; Kawasaki, M. Electric-Field Control of Anomalous and Topological Hall Effects in Oxide Bilayer Thin Films. *Nat Commun* **2018**, *9* (1), 213. https://doi.org/10.1038/s41467-017-02629-3.
(33) Gu, Y.; Wang, Q.; Hu, W.; Liu, W.; Zhang, Z.-D.; Pan, F.; Song, C. An Overview of SrRuO3-Based Heterostructures for Spintronic and Topological Phenomena. *J. Phys. D: Appl. Phys.* **2022**. https://doi.org/10.1088/1361-6463/ac4fd3.
(34) Trier, F.; Noël, P.; Kim, J.-V.; Attané, J.-P.; Vila, L.; Bibes, M. Oxide Spin-Orbitronics: Spin–Charge Interconversion and Topological Spin Textures. *Nat Rev Mater* **2021**, 1–17. https://doi.org/10.1038/s41578-021-00395-9.
(35) Itoh, S.; Endoh, Y.; Yokoo, T.; Ibuka, S.; Park, J.-G.; Kaneko, Y.; Takahashi, K. S.; Tokura, Y.; Nagaosa, N. Weyl Fermions and Spin Dynamics of Metallic Ferromagnet SrRuO3. *Nat Commun* **2016**, *7* (1), 11788. https://doi.org/10.1038/ncomms11788.
(36) Pang, B.; Zhang, L.; Chen, Y. B.; Zhou, J.; Yao, S.; Zhang, S.; Chen, Y. Spin-Glass-Like Behavior and Topological Hall Effect in SrRuO3/SrIrO3 Superlattices for Oxide Spintronics Applications. *ACS Appl. Mater. Interfaces* **2017**, *9* (3), 3201–3207. https://doi.org/10.1021/acsami.7b00150.
(37) Zheng, D.; Fang, Y.-W.; Zhang, S.; Li, P.; Wen, Y.; Fang, B.; He, X.; Li, Y.; Zhang, C.; Tong, W.; Mi, W.; Bai, H.; Alshareef, H. N.; Qiu, Z. Q.; Zhang, X. Berry Phase Engineering in SrRuO3/SrIrO3/SrTiO3 Superlattices Induced by Band Structure Reconstruction. *ACS Nano* **2021**, *15* (3), 5086–5095. https://doi.org/10.1021/acsnano.0c10200.
(38) Yang, L.; Wysocki, L.; Schöpf, J.; Jin, L.; Kovács, A.; Gunkel, F.; Dittmann, R.; van Loosdrecht, P. H. M.; Lindfors-Vrejoiu, I. Origin of the Hump Anomalies in the Hall Resistance Loops of Ultrathin ${\mathrm{SrRuO}}_{3}/{\mathrm{SrIrO}}_{3}$ Multilayers. *Phys. Rev. Materials* **2021**, *5* (1), 014403. https://doi.org/10.1103/PhysRevMaterials.5.014403.
(39) Gu, Y.; Song, C.; Zhang, Q.; Li, F.; Tan, H.; Xu, K.; Li, J.; Saleem, M. S.; Fayaz, M. U.; Peng, J.; Hu, F.; Gu, L.; Liu, W.; Zhang, Z.; Pan, F. Interfacial Control of Ferromagnetism in Ultrathin SrRuO3 Films Sandwiched between Ferroelectric BaTiO3 Layers. *ACS Appl. Mater. Interfaces* **2020**, *12* (5), 6707–6715. https://doi.org/10.1021/acsami.9b20941.
(40) Wang, L.; Feng, Q.; Kim, Y.; Kim, R.; Lee, K. H.; Pollard, S. D.; Shin, Y. J.; Zhou, H.; Peng, W.; Lee, D.; Meng, W.; Yang, H.; Han, J. H.; Kim, M.; Lu, Q.; Noh, T. W. Ferroelectrically Tunable Magnetic Skyrmions in Ultrathin Oxide Heterostructures. *Nature Mater* **2018**, *17* (12), 1087–1094. https://doi.org/10.1038/s41563-018-0204-4.
(41) Yao, X.; Wang, C.; Guo, E.-J.; Wang, X.; Li, X.; Liao, L.; Zhou, Y.; Lin, S.; Jin, Q.; Ge, C.; He, M.; Bai, X.; Gao, P.; Yang, G.; Jin, K. Ferroelectric Proximity Effect and Topological Hall Effect in SrRuO3/BiFeO3 Multilayers. *ACS Appl. Mater. Interfaces* **2022**, *14* (4), 6194–6202. https://doi.org/10.1021/acsami.1c21703.
(42) Gu, Y.; Wei, Y.-W.; Xu, K.; Zhang, H.; Wang, F.; Li, F.; Saleem, M. S.; Chang, C.-Z.; Sun, J.; Song, C.; Feng, J.; Zhong, X.; Liu, W.; Zhang, Z.; Zhu, J.; Pan, F. Interfacial Oxygen-Octahedral-Tilting-

Driven Electrically Tunable Topological Hall Effect in Ultrathin SrRuO3 Films. *J. Phys. D: Appl. Phys.* **2019**, *52* (40), 404001. https://doi.org/10.1088/1361-6463/ab2fe8.

(43) Ziese, M.; Jin, L.; Lindfors-Vrejoiu, I. Unconventional Anomalous Hall Effect Driven by Oxygen-Octahedra-Tailoring of the SrRuO3 Structure. *J. Phys. Mater.* **2019**, *2* (3), 034008. https://doi.org/10.1088/2515-7639/ab1aef.

(44) Lindfors-Vrejoiu, I.; Ziese, M. Topological Hall Effect in Antiferromagnetically Coupled SrRuO3/La0.7Sr0.3MnO3 Epitaxial Heterostructures. *physica status solidi (b)* **2017**, *254* (5), 1600556. https://doi.org/10.1002/pssb.201600556.

(45) Ziese, M.; Bern, F.; Esquinazi, P. D.; Lindfors-Vrejoiu, I. Topological Signatures in the Hall Effect of SrRuO3/La0.7Sr0.3MnO3 SLs. *physica status solidi (b)* **2020**, *257* (7), 1900628. https://doi.org/10.1002/pssb.201900628.

(46) Kan, D.; Moriyama, T.; Kobayashi, K.; Shimakawa, Y. Alternative to the Topological Interpretation of the Transverse Resistivity Anomalies in ${\mathrm{SrRuO}}_{3}$. *Phys. Rev. B* **2018**, *98* (18), 180408. https://doi.org/10.1103/PhysRevB.98.180408.

(47) Kimbell, G.; Sass, P. M.; Woltjes, B.; Ko, E. K.; Noh, T. W.; Wu, W.; Robinson, J. W. A. Two-Channel Anomalous Hall Effect in ${\mathrm{SrRuO}}_{3}$. *Phys. Rev. Materials* **2020**, *4* (5), 054414. https://doi.org/10.1103/PhysRevMaterials.4.054414.

(48) Kimbell, G.; Kim, C.; Wu, W.; Cuoco, M.; Robinson, J. W. A. Challenges in Identifying Chiral Spin Textures via the Topological Hall Effect. *Commun Mater* **2022**, *3* (1), 1–18. https://doi.org/10.1038/s43246-022-00238-2.

(49) Roy, P.; Carr, A.; Zhou, T.; Paudel, B.; Wang, X.; Chen, D.; Kang, K. T.; Pateras, A.; Corey, Z.; Lin, S.; Zhu, J.-X.; Holt, M. V.; Yoo, J.; Zapf, V.; Zeng, H.; Ronning, F.; Jia, Q.; Chen, A. Origin of Topological Hall-Like Feature in Epitaxial SrRuO3 Thin Films. *Advanced Electronic Materials n/a* (n/a), 2300020. https://doi.org/10.1002/aelm.202300020.

(50) Deng, H.; Yang, C. P.; Zhou, Z. H.; Wang, H.; Baerner, K.; Medvedeva, I. V. Electroresistance Effect in La1−xCaxMnO3 (0. *Journal of Physics and Chemistry of Solids* **2010**, *71* (12), 1660–1663. https://doi.org/10.1016/j.jpcs.2010.08.015.

(51) Dowden, P. C.; Bi, Z.; Jia, Q. X. Method for Controlling Energy Density for Reliable Pulsed Laser Deposition of Thin Films. *Review of Scientific Instruments* **2014**, *85* (2), 025111. https://doi.org/10.1063/1.4865716.

(52) Chen, A.; Su, Q.; Han, H.; Enriquez, E.; Jia, Q. Metal Oxide Nanocomposites: A Perspective from Strain, Defect, and Interface. *Advanced Materials* **2019**, *31* (4), 1803241. https://doi.org/10.1002/adma.201803241.

(53) Herranz, G.; Martínez, B.; Fontcuberta, J.; Sánchez, F.; Ferrater, C.; García-Cuenca, M. V.; Varela, M. Enhanced Electron-Electron Correlations in Nanometric ${\mathrm{SrRuO}}_{3}$ Epitaxial Films. *Phys. Rev. B* **2003**, *67* (17), 174423. https://doi.org/10.1103/PhysRevB.67.174423.

(54) Tian, D.; Liu, Z.; Shen, S.; Li, Z.; Zhou, Y.; Liu, H.; Chen, H.; Yu, P. Manipulating Berry Curvature of SrRuO3 Thin Films via Epitaxial Strain. *PNAS* **2021**, *118* (18). https://doi.org/10.1073/pnas.2101946118.

(55) Qin, Q.; Liu, L.; Lin, W.; Shu, X.; Xie, Q.; Lim, Z.; Li, C.; He, S.; Chow, G. M.; Chen, J. Emergence of Topological Hall Effect in a SrRuO3 Single Layer. *Advanced Materials* **2019**, *31* (8), 1807008. https://doi.org/10.1002/adma.201807008.

(56) Wang, C.; Chang, C.-H.; Herklotz, A.; Chen, C.; Ganss, F.; Kentsch, U.; Chen, D.; Gao, X.; Zeng, Y.-J.; Hellwig, O.; Helm, M.; Gemming, S.; Chu, Y.-H.; Zhou, S. Topological Hall Effect in Single Thick SrRuO3 Layers Induced by Defect Engineering. *Advanced Electronic Materials* **2020**, *6* (6), 2000184. https://doi.org/10.1002/aelm.202000184.

(57) Meng, K.-Y.; Ahmed, A. S.; Baćani, M.; Mandru, A.-O.; Zhao, X.; Bagués, N.; Esser, B. D.; Flores, J.; McComb, D. W.; Hug, H. J.; Yang, F. Observation of Nanoscale Skyrmions in SrIrO3/SrRuO3 Bilayers. *Nano Lett.* **2019**, *19* (5), 3169–3175. https://doi.org/10.1021/acs.nanolett.9b00596.

(58) Swekis, P.; Markou, A.; Kriegner, D.; Gayles, J.; Schlitz, R.; Schnelle, W.; Goennenwein, S. T. B.; Felser, C. Topological Hall Effect in Thin Films of ${\mathrm{Mn}}_{1.5}\mathrm{PtSn}$. *Phys. Rev. Materials* **2019**, *3* (1), 013001. https://doi.org/10.1103/PhysRevMaterials.3.013001.
(59) Ludbrook, B. M.; Dubuis, G.; Puichaud, A.-H.; Ruck, B. J.; Granville, S. Nucleation and Annihilation of Skyrmions in Mn2CoAl Observed through the Topological Hall Effect. *Sci Rep* **2017**, *7* (1), 13620. https://doi.org/10.1038/s41598-017-13211-8.
(60) Huang, M.; Gao, L.; Zhang, Y.; Lei, X.; Hu, G.; Xiang, J.; Zeng, H.; Fu, X.; Zhang, Z.; Chai, G.; Peng, Y.; Lu, Y.; Du, H.; Chen, G.; Zang, J.; Xiang, B. Possible Topological Hall Effect above Room Temperature in Layered Cr1.2Te2 Ferromagnet. *Nano Lett.* **2021**, *21* (10), 4280–4286. https://doi.org/10.1021/acs.nanolett.1c00493.
(61) Gerber, A. Interpretation of Experimental Evidence of the Topological Hall Effect. *Phys. Rev. B* **2018**, *98* (21), 214440. https://doi.org/10.1103/PhysRevB.98.214440.
(62) Grutter, A.; Wong, F.; Arenholz, E.; Liberati, M.; Suzuki, Y. Enhanced Magnetization in Epitaxial SrRuO3 Thin Films via Substrate-Induced Strain. *Journal of Applied Physics* **2010**, *107* (9), 09E138. https://doi.org/10.1063/1.3360345.
(63) Liu, J.; Feng, Y.; Tang, R.; Zhao, R.; Gao, J.; Shi, D.; Yang, H. Mechanically Tunable Magnetic Properties of Flexible SrRuO3 Epitaxial Thin Films on Mica Substrates. *Advanced Electronic Materials* **2018**, *4* (4), 1700522. https://doi.org/10.1002/aelm.201700522.
(64) Zahradník, M.; Uhlířová, K.; Maroutian, T.; Kurij, G.; Agnus, G.; Veis, M.; Lecoeur, P. Magnetic Domain Wall Motion in SrRuO3 Thin Films. *Materials & Design* **2020**, *187*, 108390. https://doi.org/10.1016/j.matdes.2019.108390.
(65) Gao, R.; Dong, Y.; Xu, H.; Zhou, H.; Yuan, Y.; Gopalan, V.; Gao, C.; Fong, D. D.; Chen, Z.; Luo, Z.; Martin, L. W. Interfacial Octahedral Rotation Mismatch Control of the Symmetry and Properties of SrRuO3. *ACS Appl. Mater. Interfaces* **2016**, *8* (23), 14871–14878. https://doi.org/10.1021/acsami.6b02864.